2008

An Experimental Technique for the Evaluation of Strain Dependent Material Properties of Hard Coatings

Shad A. Reed

Anthony N. Palazotto
Air Force Institute of Technology

William P. Baker
Air Force Institute of Technology

Shock and Vibration 15 (2008) 697–712
IOS Press

An experimental technique for the evaluation of strain dependent material properties of hard coatings

Shad A. Reed[a,*], Anthony N. Palazotto[a] and William P. Baker[b]
[a]*Department of Aeronautics and Astronautics: Air Force Institute of Technology, 2950 Hobson Way, Building 640, WPAFB, OH 45433-7765, USA*
[b]*Department of Mathematics and Statistics: Air Force Institute of Technology, 2950 Hobson Way, Building 640, WPAFB, OH 45433-7765, USA*

Received 3 July 2007
Revised 17 October 2007

Abstract. A novel vibration experiment consisting of a free-free boundary condition, an electromagnetic excitation source, a vacuum chamber, and a laser vibrometer based surface measurement system has been developed that permits high levels of excitation on highly damped specimens with a minimal amount of unwanted systematic error. While some of the aspects of this experiment are not unique, when combined with a processing technique that accounts for the nonlinearities present in the system, this experiment permits, accurate measurement of strain dependent stiffness and damping properties of hard coatings at high strain levels. This procedure has been demonstrated using a titanium beam that has been coated with a free-layer damping treatment of Magnesium Aluminate Spinel. The results indicate that Magnesium Aluminate Spinel has both nonlinear stiffness and damping properties. The stiffness asymptotes to a minimum value around 650 microstrain while the damping is a maximum around 100 microstrain. Additionally, the data contained herein cover a larger strain range for this material than previously reported.

Keywords: Nonlinear damping, nonlinear stiffness, free-free boundary condition, Hilbert Transform, hard coatings, magnesium aluminate spinel

1. Introduction

High Cycle Fatigue (HCF) is a broad classification for a failure that occurs when a vibratory stress lower than the elastic limit is applied to a structure over a large number of cycles and results in the failure of a component. In turbine engines, vibratory stress is a function of the rotational frequencies of engine components, aeromechanical loading, and the material properties of the components. In 1992, the USAF Scientific Advisory Board concluded that High Cycle Fatigue (HCF) was the leading single cause of turbine engine failure. In an effort to prevent high cycle fatigue of turbine engine blades, manufacturers have investigated several ways to reduce vibratory stress and increase a component's ability to withstand these stresses. Increasing the damping associated with a structure can decrease stress amplitudes and provide extended life. While viscoelastic treatments such as constrained layer dampers offer a significant amount of damping, they are not well suited for the hostile environment of a turbine engine due to their strong temperature dependence. Alternatively, so called hard coatings have received attention in recent years because they are relatively easy to apply, provide reasonable amounts of damping, and display reduced dependence on temperature. Unfortunately, the stiffness and damping of materials in this class have been shown to

*Corresponding author. Tel.: +1 937 255 3636 ext 7455; Fax: +1 937 656 7053; E-mail: anthony.palazotto@afit.edu.

ISSN 1070-9622/08/$17.00

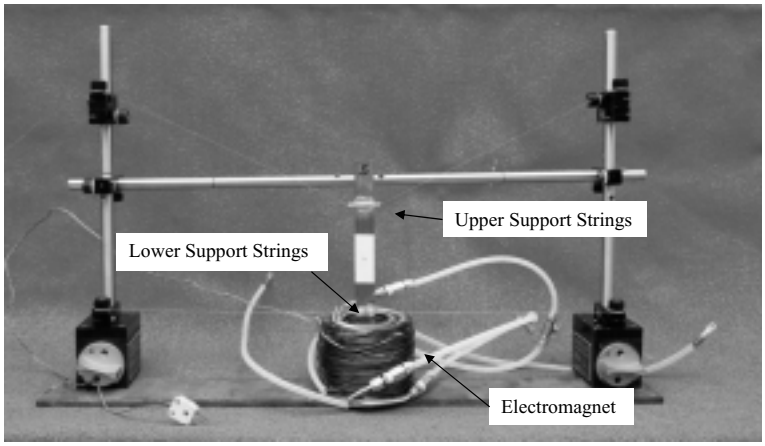

Fig. 1. Beam support system.

have a nonlinear dependence on strain. For this and other reasons, it is often difficult to find reliable and repeatable data that adequately captures the nonlinear, strain dependent nature of the stiffness and damping properties of hard coatings.

2. Experimental method

The goal of this effort is to quantify the stiffness and damping of a nonlinear material. Because the material is a sprayed on coating, it is not possible to test the response of monolithic specimens of the material. Therefore, the material properties will be determined by comparing the response, specifically the instantaneous resonant frequency and loss factor, of two systems, one with the coating and one without the coating in a manner similar to that offered by Torvik [1]. Because the amount of damping contributed to a system by a hard coating can be rather small, it is critical that the experimental procedure be designed in such a way as to accentuate the influence of the coating on the system. In general this is accomplished by having an uncoated system with a constant resonant frequency and extremely low baseline damping.

3. Setup

In order to ensure that the energy dissipation in the coated system was primarily due to the coating, it was decided that the experiment be conducted in a vacuum chamber, thereby minimizing any damping associated with the beam vibrating in a viscous medium. The vacuum chamber used in this study was capable of achieving pressures of 20 mm Hg. Additionally, it was decided that a free-free boundary condition should be used, effectively eliminating energy dissipation present in the clamps required to simulate a cantilevered or fixed boundary condition. The free-free boundary condition was approximated by suspending the beam vertically from the upper node of the first mode using fine gauge nylon string as seen in Fig. 1. A pair of nylon strings was also placed at the lower node of the beam to minimize unwanted rigid body motion. By placing the support and guide wires at the nodal locations, they are held relatively motionless and do not contribute to the dynamics of the system.

The free-free boundary condition complicates the excitation and measurement of the beam. Beam excitation is achieved using a custom built, water cooled, electromagnet driven by a sinusoidal signal generated by a function generator and amplified by an MB Dynamics SL600VCF Power Amplifier. This system was developed by Runyon et al. [2]. The current from the amplifier produces an oscillating magnetic field around the electromagnet that creates a couple on a pair of small permanent rare-earth magnets glued to the lower node of the beam specimen as shown in Fig. 2. By placing the magnets at the lower node of the beam, the magnets do not undergo significant translations and therefore do not enter into the dynamics of the beam. Beam excitation was measured using a single point Polytec

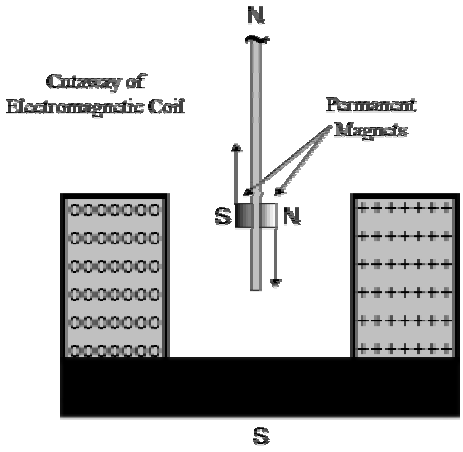

Fig. 2. Electromagnetic excitation.

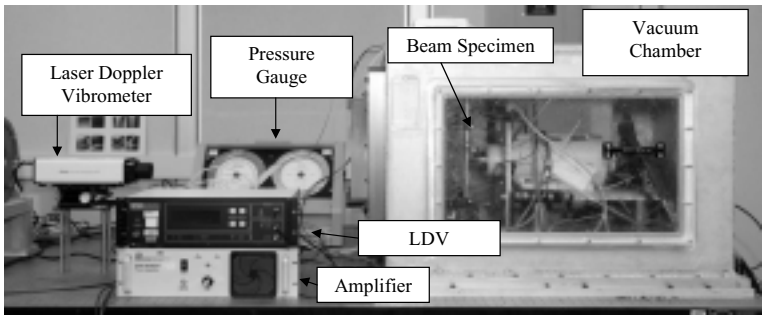

Fig. 3. Overview of experimental setup.

OFV-303 Laser Doppler Vibrometer (LDV) capable of measuring velocities up to 10 m/s. The ability of the LDV to measure velocities up to this limit is critical for capturing high strain data. The entire experimental setup can be seen in Fig. 3.

3.1. Specimen description

Two beam specimens were cut from 1.59 mm thick Ti-6Al-4V sheet stock. The finished dimensions of both beams was 19.0 mm $\times$ 200 mm $\times$ 1.59 mm. The coated beam was coated on both faces over the center 36.5% of the beam with 0.25 mm of Magnesium Aluminate Spinel as shown in Fig. 4. Because the material properties of the coating material are known to depend on strain, it is necessary to minimize the amount of length-wise strain variation in the coating.

3.2. Experimental procedure

It has been shown by a number of researchers [3–5] that hard coatings such as Magnesium Aluminate Spinel have nonlinear material properties, that is, the stiffness and damping depend on the strain in the material. Therefore, the experiment must be capable of capturing this behavior. While both frequency and time domain based experimental techniques have been shown by Torvik and Patsias [4] to yield similar estimates of system loss factor for specimens with weakly nonlinear material properties, a time domain approach has been pursued in this research. Frequency domain techniques generally apply an excitation signal whose amplitude is controlled such that either the system response or the amplitude of the excitation is held constant as the frequency of the excitation is swept through a given range. For linear systems, this process only needs to be done for one level of system response. However, for systems

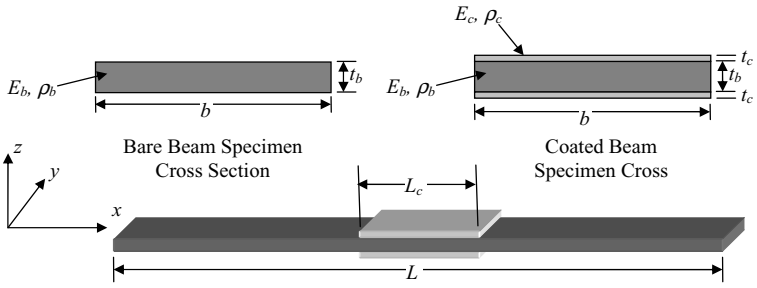

Fig. 4. Beam specimens.

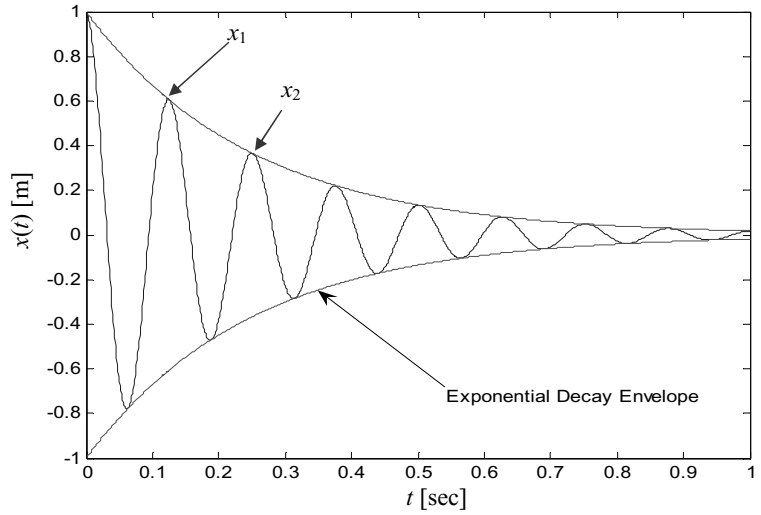

Fig. 5. Free decay of a damped single degree of freedom system.

displaying amplitude dependent characteristics, the test must be conducted for several different response amplitudes or excitation amplitudes in order to fully characterize the system. In contrast, a time domain based approach uses the free decay of a system from a known state in order to find the stiffness and damping of the system. If the system is linear, the entire decay will indicate constant values for the system stiffness and damping. However, if the system is nonlinear, the single free decay signal will provide a continuously varying record of the system stiffness and damping for all amplitudes thereby providing much more information with minimal experimentation.

3.3. Data processing

A typical time domain based experiment records the free response of a system to an initial condition as a function of time and then uses the decay of the system to determine the damping present in the system. The most commonly used technique is the log decrement method. Figure 5 shows the free response of a typical single degree of freedom spring-mass-damper system that was released from an initial displacement, $x\left(0\right) = 1$ m, and an initial velocity, $\dot{x}\left(0\right) = 0$ m/s.

This system can be described with the following differential equation of motion.

$$m\ddot{x} + c\dot{x} + kx = 0 \tag{1}$$

In general, the solution of this equation is

$$x\left(t\right) = Ae^{-\zeta\omega t}\cos\left(\omega_d t\right) \tag{2}$$

where A is the initial displacement, x(0)=A, ζ is the damping ratio, ω is the undamped natural frequency and ω_d is the damped natural frequency. The log decrement, Λ, is calculated using successive peaks on the decay, shown as x_1 and x_2 in Fig. 5. These two peaks have amplitudes equal to:

$$x_1 = Ae^{-\zeta\omega t} \tag{3}$$

$$x_2 = Ae^{-\zeta\omega(t+T)} \tag{4}$$

where $T = \frac{2\pi}{\omega_d}$. The log decrement is found by taking the natural logarithm of the ratio of these two quantities,

$$\Lambda = \ln\frac{x_1}{x_2} = \ln\frac{Ae^{-\zeta\omega t}}{Ae^{-\zeta\omega(t+T)}} = \zeta\omega T \tag{5}$$

Because the damped and undamped natural frequencies [6] are related by

$$\omega_d = \omega\sqrt{1-\zeta^2} \tag{6}$$

Equation (5) can also be written

$$\Lambda = \zeta\omega\left(\frac{2\pi}{\omega_d}\right) = \zeta\omega\left(\frac{2\pi}{\omega\sqrt{1-\zeta^2}}\right) = \zeta\left(\frac{2\pi}{\sqrt{1-\zeta^2}}\right) \tag{7}$$

For values of $\zeta < 0.25$, this expression can be approximated using Eq. (8).

$$\Lambda \cong 2\pi\zeta \tag{8}$$

Note that Eq. (7) is valid for all damping ratios while Eq. (8) is only valid for small damping ratios. This method is extremely easy to use and provides a reasonable estimate of the damping present in a system. For very lightly damped systems, x1 and x2 are very similar which can lead to an unacceptable amount of uncertainty in the calculation of the decrement. In these cases, it is customary to use two non-successive peaks. In this case, Eq. (5) can be written

$$\Lambda = \ln\frac{x_1}{x_n} = \ln\frac{Ae^{-\zeta\omega t}}{Ae^{-\zeta\omega(t+nT)}} = \zeta\omega nT \tag{9}$$

where n refers to the nth peak. The implication is that regardless of whether successive or non-successive peaks are used, the same damping ratio will be predicted. It is important to note, that this series of expressions was derived assuming a linear viscous damping model and it is not strictly applicable to systems not displaying linear viscous damping. Nonetheless, Runyon applied the log decrement method to a system displaying nonlinear energy dissipation mechanisms using a sliding window approach [2,3]. In this study, a value for damping ratio, ζ is calculated using n number of peaks and then a new damping ratio is evaluated using the next n number of peaks as shown in Fig. 6. The result of this sort of technique is a plot that shows how the damping ratio changes over time or, more importantly, how the damping ratio changes as a function of amplitude.

While the n-peak log decrement method is straightforward and easy to implement, it is not without its faults. First, it relies heavily on accurately identifying the exact peak of the oscillation. In practice, the continuous motion of the system is discretized through the digital data acquisition process and the true peak is never precisely recorded. The result is that there is an uncertainty associated with the decrement calculation. In order to minimize this uncertainty, either the number of data points per cycle can be maximized thereby ensuring that the peak recorded value is closer to the true peak or the number of peaks used can be increased which has the tendency to minimize the impact of small measurement errors. Unfortunately, for a nonlinear system, using a large number of peaks to calculate the decrement tends to smooth the data and mask the dependence of the decrement on amplitude. Another possibility is to use some sort of curve fitting routine to find an analytical model of each peak and then differentiate that function to find the maximum. However, the most convenient method is to apply the Hilbert Transform to the data.

The Hilbert Transform offers an alternate method to process time domain data. This method was first applied to vibration problems in 1984 by Simon and Tomlinson [7]. Since that time, over 150 articles have been published discussing the application of the Hilbert Transform to linear and non-linear vibration problems. The Hilbert Transform [8] of a real valued function $x(t)$ is defined by the integral transform

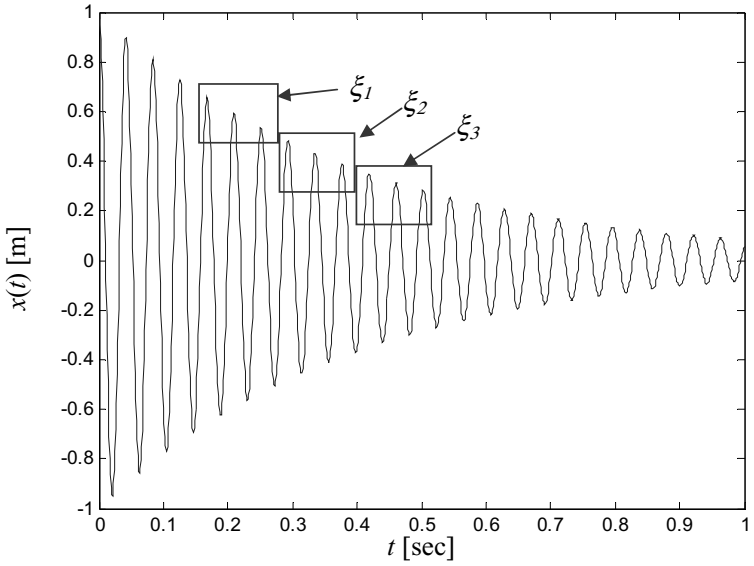

Fig. 6. Application of log decrement method to nonlinear damping.

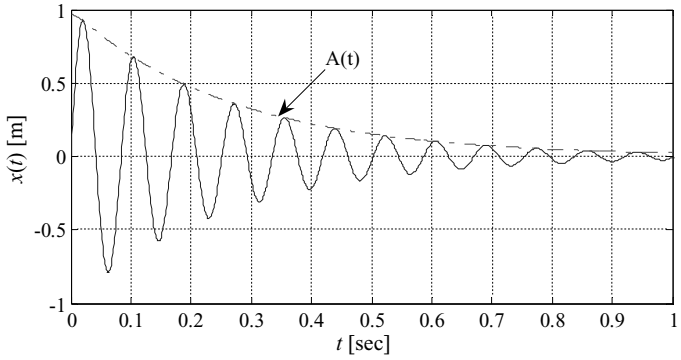

Fig. 7. Envelope of $x(t)$.

$$H\left[x\left(t\right)\right] = \tilde{x}\left(t\right) = \frac{1}{\pi}\int_{-\infty}^{\infty}\frac{x\left(\tau\right)}{t-\tau}d\tau \tag{10}$$

The integral in Eq. (10) must be considered as a Cauchy principal value to avoid the singularity at $\tau = t$. By taking the Hilbert transform of a set of real valued experimental data, an imaginary component is produced. The real and imaginary components form an analytical signal, $X\left(t\right) = x\left(t\right) + i\tilde{x}\left(t\right)$. Then by taking the modulus of the analytical signal, as shown in Eq. (11), the instantaneous amplitude of the signal can be found as shown in Fig. 7. The instantaneous amplitude is often referred to as the envelope of the signal.

$$A\left(t\right) = \left|X\left(t\right)\right| = \sqrt{x\left(t\right)^2 + \tilde{x}\left(t\right)^2} \tag{11}$$

While a traditional peak finding method is useful, it only describes the decay of a signal by tracking the peaks of the signal and discards the vast majority of the data. By taking the Hilbert Transform of a signal $x(t)$ with m number of data points, the envelope of $x(t)$, $A(t)$ will be described by m number of points, thereby drastically reducing the effect of an error in measurement of any one point. Now that the envelope has been found, the decrement can be found. In this case, the decrement is formed from two points that are not peaks of $x(t)$ but rather adjacent points on the $A(t)$ curve, therefore the time constant is $\Delta(t)$ rather than the period of oscillation.

$$\Lambda = \ln \frac{X_1}{X_2} = \ln \frac{X e^{-\zeta \omega t}}{X e^{-\zeta \omega (t+\Delta t)}} = \zeta \omega \Delta t \tag{12}$$

Now, because the damping ratio, ζ, and the loss factor, η, are related by $\eta = 2\zeta$ for small values of ζ, Eq. (12) can be rewritten

$$\Lambda = \ln \frac{X_1}{X_2} = \frac{\eta}{2} \omega \Delta t \tag{13}$$

Solving for the loss factor yields

$$\eta = \frac{2\Lambda}{\omega \Delta t} \tag{14}$$

Note that the loss factor, eta, is generally associated with a complex modulus approach where the modulus can be written $E^* = E\,(1 + i\eta)$ [9].

The Hilbert Transform also allows the determination of the instantaneous frequency of $x(t)$. For linear systems, this is not of great importance as the frequency will remain fixed and can be easily evaluated by identifying the period of oscillation. For nonlinear systems, the frequency depends on the amplitude. In order to find the frequency, the phase of the analytical signal, $X(t)$, must first be found according to Eq. (15).

$$\varphi\,(t) = \tan^{-1}\left(\frac{\tilde{x}\,(t)}{x\,(t)}\right) \tag{15}$$

Next the instantaneous circular frequency, $\omega(t)$, can be found by taking the derivative of the phase with respect to time. Recall that the circular frequency has units of rads/sec and is related to the frequency of oscillation, f, by $\omega = 2\pi f$. However, because numerical differentiation of a set of discrete points can lead to an excessively noisy result, a cubic polynomial curvefit of the phase was performed. The resulting cubic polynomial was then differentiated. Because the slope of the phase appears to be nearly constant, a cubic polynomial is able to sufficiently capture the behavior of the phase.

The instantaneous circular frequency is an important quantity because it can be used to calculate the stiffness of the system presuming the appropriate differential equation of motion is known. Since this experiment is concerned with characterizing the behavior of a system comprised of nonlinear materials operating at high strain levels, both geometric and material nonlinearities must be addressed. A study was conducted to assess the effect of the geometric nonlinearities on a free-free beam vibrating at high amplitudes. Using the experimental procedures and equipment described previously, the resonant frequency of a coated and a bare beam was plotted versus the strain amplitude at the beam-coating interface. Figure 8 indicates that the system displays negligible geometric softening at high strain amplitudes because the resonant frequency of the bare beam varies by only 0.16 Hz, or 0.07%, over the entire strain range. By comparison, the resonant frequency of the coated beam systems varies by roughly 4.3 Hz, or 1.8%. It is assumed that the coated beam system would possess the same geometric nonlinearities as the uncoated beam and an additional nonlinearity associated with the coating material. In a rough sense, the relative strengths of the nonlinearities can be evaluated. These results suggest that the material nonlinearities are at least an order of magnitude stronger than the geometric nonlinearities. For this reason, the following development will neglect the geometric nonlinearities.

After determining the system resonant frequency and loss factor, it is important to reference these values to their corresponding strain amplitude. The first step in finding the strain is the calculation of the displacement of the center of the beam located at x_0 using the velocity signal produced by the LDV and the resonant frequency as determined previously as seen in Eq. (16).

$$w\,(x_o, t) = \frac{v\,(x_o, t)}{\omega\,(t)} \tag{16}$$

In this equation, $v(x,t)$ and $w(x,t)$ refer to the velocity and displacement in the z-direction shown in Fig. 4. The second step is to determine the mode shape of the beam. If the coating fully covers the beam with a uniform thickness, t_c, then it is likely that the mode shape for the coated beam is extremely close to that of an ideal Euler Bernoulli beam and thus an analytical expression relating transverse displacement, $w(x)$, to strain, $\varepsilon(x,z)$ can be found [10].

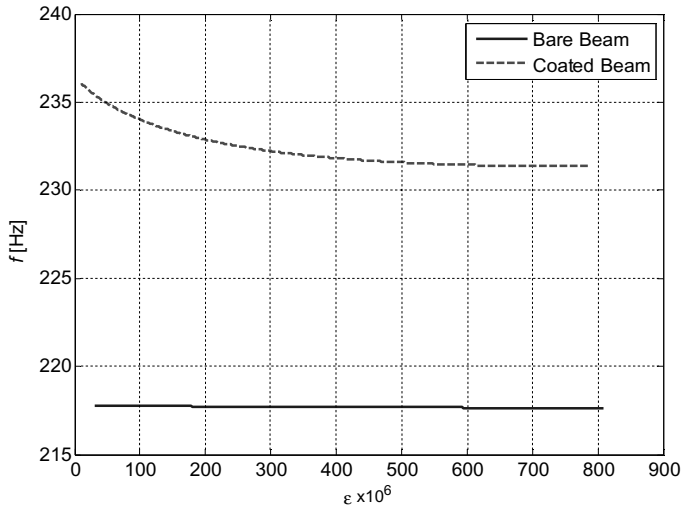

Fig. 8. Frequency variation in bare beam.

However, if the beam is partially covered with the coating material as shown in Fig. 4, different methodology must be employed.

Torvik [11] offers a method based upon analytical expressions that approximate the effect of the coating on the mode shape. In the present study, a finite element based interpolation method, similar to that shown in [12], has been developed. The finite element method will be used in an inverse fashion to first find the modulus of the bare beam, E_b, then the modulus of the coating, E_c, followed by the mode shape, $X(x)$, and strain distribution, $\varepsilon(x)$, of the partially coated beam. The stiffness of the beam is related to the natural frequency of the beam. The modulus of the bare beam is found by assuming the modulus of the beam, computing the first natural frequency using finite element analysis, comparing this value to the experimentally measured resonant frequency, adjusting the modulus of the beam, and rerunning the model. This process is repeated until a sufficient level of agreement between the experimentally measured resonant frequency and the finite element model natural frequency is achieved. This procedure is shown graphically in Fig. 9, that because the damping of a bare beam is extremely low, the experimentally measured resonant frequency is indistinguishable from the undamped natural frequency of the finite element model thus allowing these two quantities to be compared. Additionally, it should be noted that the finite element method was used in this step so that the effect of the permanent magnets could be included in the analysis. Were it not for the magnets, Euler Bernoulli beam theory would be sufficient to determine the modulus from the resonant frequency.

The modulus of the coating is found in a similar fashion and some authors [12] recommend an identical method, iteratively adjusting the coating modulus until the experimentally measured resonant frequency of the coated beam matches the natural frequency predicted by finite element analysis. However, because the stiffness of the coating is suspected to be nonlinearly dependent upon strain amplitude, the resonant frequency of the coated beam system must be measured over a wide strain range. As will be detailed later, by calculating the instantaneous resonant frequency from a free decay a tremendous amount of data can be generated thus making it quite expensive and tedious to follow this iterative process. Instead, just a few finite element analyses are performed using a range of coating moduli and the computed natural frequencies form the basis for a polynomial regression relating coating modulus to natural frequency for a given set of beam and coating parameters. The resulting polynomial provides a quick and effective way of determining coating modulus for any experimentally observed resonant frequency. It should be noted that if an n-th order polynomial is desired, then $n+1$ finite element analyses must be performed. This procedure is shown graphically in Fig. 10.

Now that both the beam and coating moduli have been determined, the mode shape and displacement function can be found. Because the coating modulus will change throughout the decay, the mode shape of the beam will likewise change. In order to capture this evolution, the mode shape will be said to have both spatial dependence and

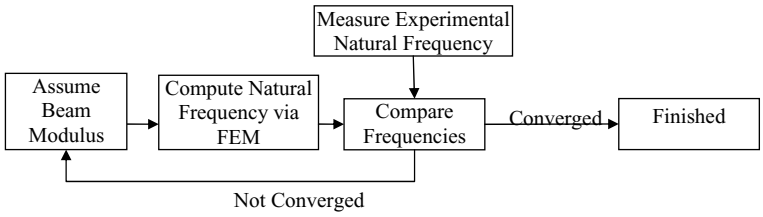

Fig. 9. Use of FEM in inverse fashion to find beam modulus.

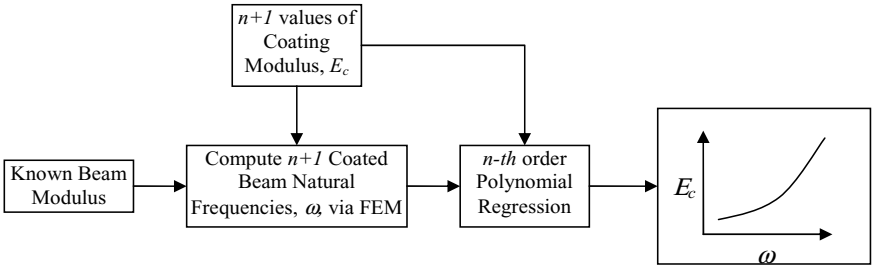

Fig. 10. Using a FEM based polynomial regression to find coating modulus.

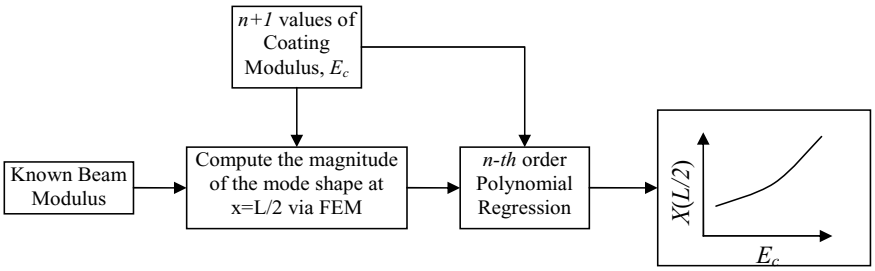

Fig. 11. Mode shape versus coating modulus.

a dependence on the strain since it is the strain amplitude that induces the change in the coating modulus. Therefore the mode shape will be denoted as $X(x, Ec(\varepsilon))$. At any time t, the displacement function, $w(x,t)$, can be related by a scaling factor, $\lambda(t)$ as seen in Eq. (17).

$$\lambda(t) = \frac{w(x,t)}{X(x, E_c(\varepsilon))} \tag{17}$$

In order to determine this scaling factor, the experimentally measured displacement at the center of the beam, $x = x_o$, will be used. The magnitude of the mode shape at this location will be found using the Finite Element Method. Because the mode shape of the coated beam depends on the coating modulus, which will be continually changing throughout a decay, the magnitude of the mode shape at $x = L/2$ corresponding to $n+1$ values of E_c will be extracted from the same models used to correlate frequency to coating modulus. Then, a polynomial will be fit to the data to provide a continuous relationship between coating modulus and the magnitude of the mode shape at $x = L/2$. This can be seen in Fig. 11. To reiterate, after experimentally measuring the coated beam resonant frequency, the coating modulus is found using the polynomial regression shown in Fig. 10. Then after the coating modulus is found, the magnitude of the mode shape at $x = L/2$ is found using the polynomial regression shown in Fig. 11. The result is a continuously varying value for the magnitude of the mode shape at x_0 for the entire decay. At this point, the scaling factor, $\lambda(t)$, can be calculated using Eq. (17).

In accordance with the precedent set by Torvik [1,16] and Patsias [5], the peak strain along the interface between the coating and the beam was used as the reference strain when reporting the material properties. Therefore, the

strain distribution along this surface will be extracted from the $n+1$ finite element analyses previously performed. Then, just as was done with the mode shape, a polynomial relating the maximum value of the strain distribution in the coated region and the coating modulus was found. The strain values extracted from the finite element analyses, $\tilde{\varepsilon}(x)$, must be rescaled since they are dependent upon a normalized mode shape. The actual strain, $\varepsilon(x)$, can be found using the same scaling factor found in Eq. (17) because strain is linearly dependent on the curvature of the displacement as seen in Eq. (18).

$$\varepsilon(x,t_b,t) = \lambda(t)\,\tilde{\varepsilon}(x) = t_b \frac{\partial^2 w(x,t)}{\partial x^2} = t_b \lambda(t)\,\frac{\partial^2 X(x,t)}{\partial x^2} \tag{18}$$

As stated, the goal of this experiment is to determine the material properties of a coating from the response of two systems, one that includes the coating and one that does not. At this point, the dependence of two system level properties, resonant frequency and loss factor, on strain has been determined. Through a finite element based method, the coating modulus has been determined and associated with a particular reference strain. The final step is to determine the loss factor of the coating.

In order to isolate the material loss factor of the coating, we utilize the definition of the system loss factor, η_{sys}, which is shown in Eq. (19) [1].

$$\eta_{sys} = \frac{1}{2\pi}\frac{D_{sys}}{U_{sys}} \tag{19}$$

where Dsys and Usys are the energy dissipated and stored in the system per cycle respectively. There are several sources of energy dissipation in a system. In the case of a bare vibrating beam, these include the fixture or boundary conditions (D_f), the interaction of the specimen with the fluid surrounding it (D_a), and the internal friction present in beam (D_b). Therefore the system damping can be represented by Eq. (20).

$$D_{sys} = D_f + D_a + D_b \tag{20}$$

Likewise, the stored energy in the system is a summation of the energy stored in the beam (U_b) and the boundary (U_f). This can be represented by Eq. (21).

$$U_{sys} = U_f + U_b \tag{21}$$

Now substituting Eqs (20) and (21) into Eq. (19), we arrive at the following expression for the system loss factor for a bare beam, η_{bare}.

$$\eta_{\mathrm{bare}} = \frac{1}{2\pi}\frac{D_f + D_a + D_b}{U_f + U_b} \tag{22}$$

The addition of a damping treatment will introduce contributions to both the stored energy and the energy dissipation. The system loss factor for a coated beam can be written

$$\eta_{sys} = \frac{1}{2\pi}\frac{D'_f + D'_a + D'_b + D_c}{U'_f + U'_b + U_c} \tag{23}$$

The primes in Eq. (23) are used to recognize that while these quantities also exist in Eq. (22), they may not be identical due to the influence of the coating on the mode shape of the coated beam. Equation (23) can also be rewritten

$$\eta_{sys} = \frac{1}{2\pi}\frac{D_c}{U'_f + U'_b + U_c} + \frac{1}{2\pi}\frac{D'_f + D'_a + D'_b}{U'_f + U'_b + U_c} \tag{24}$$

or

$$\eta_{sys} = \frac{1}{2\pi}\frac{\frac{D_c}{U_c}}{\frac{U'_f + U'_b}{U_c} + 1} + \frac{1}{2\pi}\frac{\frac{D'_f + D'_a + D'_b}{U'_f + U'_b}}{\frac{U_c}{U'_f + U'_b} + 1} \tag{25}$$

If the bare beam system displays a linear loss factor, then it can be assumed that the loss factor of the bare beam, Eq. (22), is negligibly different from the numerator of the second term in Eq. (24). In other words,

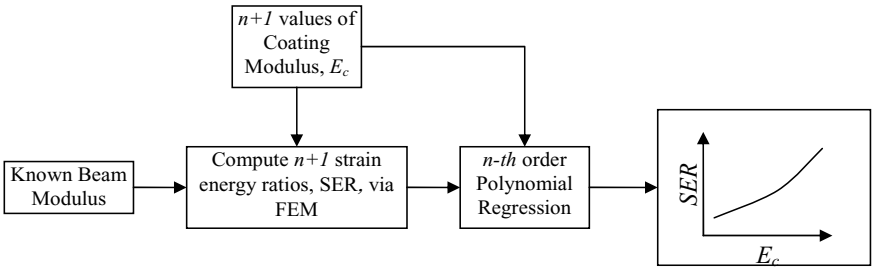

Fig. 12. Polynomial relating strain energy to coating modulus.

$$\frac{1}{2\pi}\frac{D_f + D_a + D_b}{U_f + U_b} \cong \frac{1}{2\pi}\frac{D'_f + D'_a + D'_b}{U'_f + U'_b} \tag{26}$$

Therefore, Eq. (22) can be substituted into Eq. (24) yielding Eq. (27).

$$\eta_{sys} = \frac{1}{2\pi}\frac{\frac{D_c}{U_c}}{\frac{U'_f+U'_b}{U_c}+1} + \frac{1}{2\pi}\frac{\frac{D_f+D_a+D_b}{U_f+U_b}}{\frac{U_c}{U'_f+U'_b}+1} \tag{27}$$

At this point, the loss factor of the material, η_{mat}, and the loss factor of the bare beam can be utilized to simplify Eq. (27).

$$\eta_{\mathrm{sys}} = \frac{\eta_{\mathrm{mat}}}{\frac{U'_f+U'_b}{U_c}+1} + \frac{\eta_{\mathrm{bare}}}{\frac{U_c}{U'_f+U'_b}+1} \tag{28}$$

Further simplification of Eq. (27) can be accomplished by assuming that the strain energy stored by the fixture, U_f, is negligible. The denominators of Eq. (27) represent strain energy ratios. By defining the ratio of strain energy in the coating to the strain energy in the beam,

$$R_{SE} = \frac{U_c}{U'_b} \tag{29}$$

we arrive at Eq. (30).

$$\eta_{sys} = \frac{\eta_{mat}}{\frac{1}{R_{SE}}+1} + \frac{\eta_{bare}}{R_{SE}+1} \tag{30}$$

Equation (30) can then be rearranged to yield an expression for the loss factor of the coating material in terms of the loss factors of the coated and uncoated systems and the strain energy ratio.

$$\eta_{mat} = \frac{\eta_{sys}\,(R_{SE}+1) - \eta_{\mathrm{bare}}}{R_{SE}} \tag{31}$$

If this system were linear, the strain energy ratio would be constant throughout the decay. However, that is not the case and the variation of the strain energy ratio must be considered. In order to do this, the ratio of strain energy stored in the beam versus the strain energy stored in the coating is extracted from the $n+1$ finite element analyses performed previously. To reiterate, these n+1 finite element analyses are identical except that each one uses a slightly different value of coating modulus. Then a polynomial relating coating modulus to strain energy ratio can be found as shown graphically in Fig. 12. Finally, the strain energy ratio can be found throughout the entire decay using the coating modulus values computed earlier.

In the end, the nonlinear coating modulus and loss factor have been extracted from the response of two beam systems, one coated and one uncoated, as the beams decay from an initial condition. The steps required to do this are listed below:

1. Measure the velocity of both beams during a decay using a laser Doppler vibrometer.
2. Apply the Hilbert Transform to find the complex part of the analytic signal.

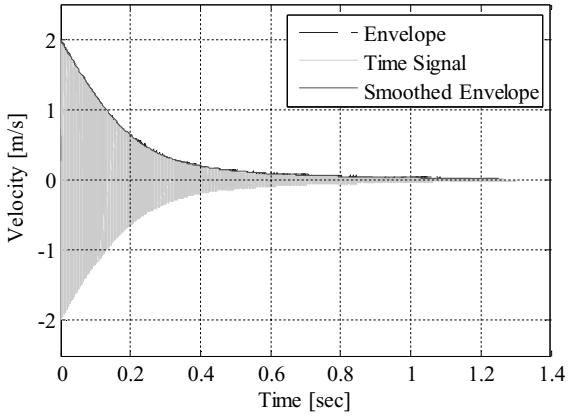

Fig. 13. Free decay of a bare beam.

3. Compute the modulus of the analytic signal to find the envelope curve. Apply smoothing techniques as necessary to eliminate the presence of extraneous frequencies and noise.
4. Using the log decrement, find the loss factor of the two systems.
5. Compute the phase of the analytic signal.
6. Differentiate the phase with respect to time to find the instantaneous frequency of the two systems.
7. Use finite element analysis to find the modulus of the bare beam from the instantaneous frequency of the bare beam.
8. Perform $n+1$ finite element analyses of coated beams comprised of $n+1$ different values of coating modulus.
9. Perform n-th order polynomial regressions relating coating modulus to the following quantities.

   a. ω vs. E_c.
   b. E_c vs. $X(L/2)$.
   c. E_c vs. $\tilde{\varepsilon}(t_b, L/2)$.
   d. E_c vs. U'_b/U_c.

10. Calculate the following quantities throughout the decay.

    a. E_c.
    b. X(L/2).
    c. $\lambda(t)$.
    d. $\varepsilon(t_b, L/2)$.
    e. U'_b/U_c.
    f. η_{mat}.

4. Results

The procedure has been applied to a Ti-6Al-4V beam measuring 19.0 mm $\times$ 200 mm $\times$ 1.59 mm coated on both sides with 0.25 mm of Magnesium Aluminate Spinel, a plasma sprayed coating originally used as a thermal barrier coating. The coating density was determined, using simple weights and measures, to be 2565 kg/m^3.

The beams were placed in a vacuum chamber operating at room temperature and a pressure of 20 mmHg. The beams were excited to a maximum response level by driving the electromagnet at the resonant frequency of the beams. Once the steady state maximum response was established, the excitation was interrupted using a feature of the wave form generator that allows the output signal to be cut abruptly. Figure 13 shows the free decay of the bare beam. The Hilbert command available in the signal processing toolbox of MATLAB was used to compute the analytical signal and thus the envelope of the velocity, $A(t)$, as shown in Fig. 14. Also shown in Fig. 14 are the results

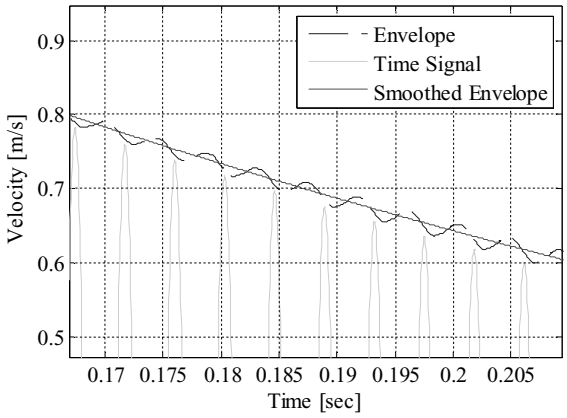

Fig. 14. Free decay of a bare beam.

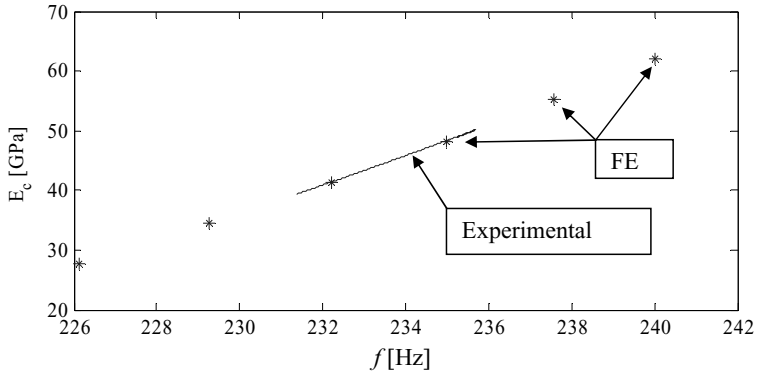

Fig. 15. Variation of coating modulus vs natural frequency.

of a MATLAB cubic smoothing spline routine, csaps, which has been applied to the envelope of a velocity signal. The cubic smoothing spline routine was necessary to smooth the effects of the noise and extraneous frequencies present in the envelope function. The extraneous frequencies have been traced to the rigid body modes associated with the simulated free-free boundary condition. This was done by visually identifying the rigid body frequencies and confirming their presence in the frequency response function.

The methods described in the previous sections were applied to determine the material properties of the coating. Six different coating moduli were used to generate the polynomials needed to relate natural frequency and mode shape to coating modulus. The coating moduli were chosen such that they fully span the range of coating modulus likely to be seen in the experiment. This is important so that the polynomial regressions are not used beyond their valid range. The polynomial regressions were performed using the polyfit command available in MATLAB while the commercial finite element program ANSYS was used to perform the modal analysis of the bare and coated beams. Figures 15 and 16 show six data points corresponding to six FEM analyses performed using different coating moduli. These two plots are representative of the types of regressions performed. It can be seen that the decays fully encompass the experimental data and that the relationships are nearly linear.

Figure 17 illustrates how the modulus of the coating varies with strain. Clearly, the modulus of the coating displays a softening material nonlinearity with a minimum value at a peak interface strain of 600 microstrain. Note that the peak interface strain is merely a reference. The actual strain in the coating can be up to 10% less than interface strain in the lengthwise direction and up to 13% greater on the outer fiber of the coating. In reference [13] Torvik reports the modulus for Magnesium Spinel to be around 42 GPa which falls in the center of the range of moduli computed using this method. It is important to note that this appears to be the only study that quantifies the stiffness

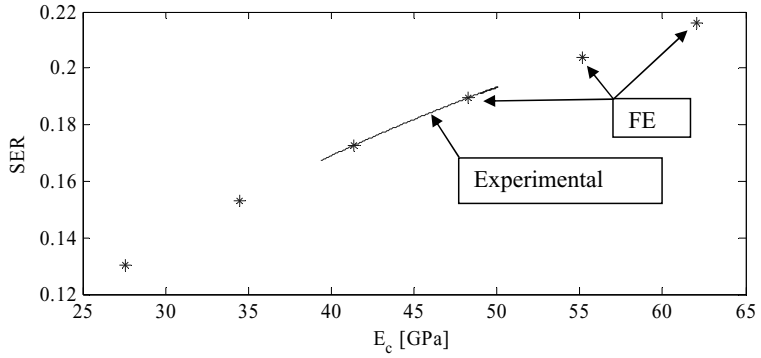

Fig. 16. Variation of strain energy ratio vs. coating modulus.

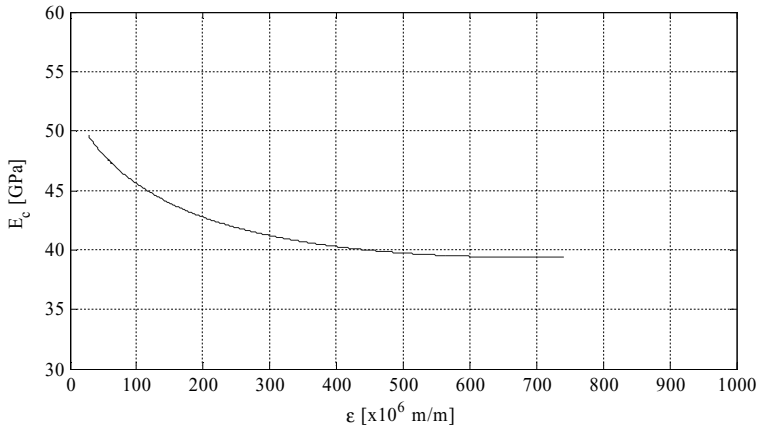

Fig. 17. Modulus of Magnesium Aluminate Spinel.

of this material. Interestingly, it also appears that the strength of the nonlinearity diminishes as the reference strain increases.

Figure 18 illustrates the loss factor, η_c, for Magnesium Aluminate Spinel. While the magnitudes of the material loss factor are consistent with results from other studies [5,14,15], they display a trend not previously seen in the literature for this material. Several studies [5,15,16] show the loss factor of the coating increasing with strain and then leveling off. The data present in this study indicate a decrease of nearly 30% after reaching a maximum value near 250 microstrain. Additionally, one of the more important aspects of this work is that the peak strain range achieved was roughly 33% greater than all other studies of this material [5,15,16].

There are numerous potential explanations for the differences in the trends. The first could be attributed to the testing methodology employed. Torvik acknowledges that experiments performed on a different coating of a similar nature were effected by whether the tests were conducted with increasing or decreasing levels of excitation [12,15]. Since these experiments were conducted using a free decay, the amplitude started high and decreased. If a forced response test were performed using a progressively higher level of excitation, the trend may have been different. Similarly, the particular coated specimen used for this work had already been subjected to several million cycles at fairly high strain level. The reason for this was that it was observed that the frequency and amplitude of the resonant response drifted by 10–20% over as the number of cycles accumulated on the specimen. The results shown here are for a specimen that displayed a stabilized resonant response. Additionally, it has been suggested that the properties of the material exhibit short term memory effects. For instance, Patsias [12] has indicated that the material properties are somewhat dependent on the initial level of excitation. Many of these concerns will be addressed and documented in subsequent publications.

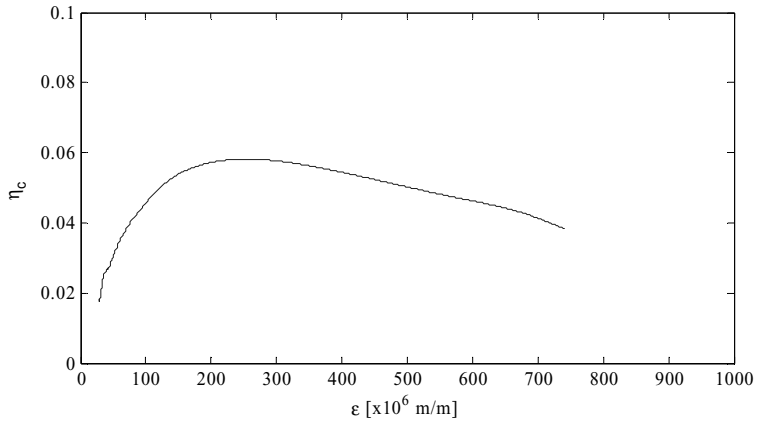

Fig. 18. Loss Factor of Magnesium Aluminate Spinel.

A final word must be said regarding the general method of differencing the response of coated and uncoated systems and then deducing the properties of the coating. Theoretically, there should be no problem with this approach. In practice though, the presence of the coating is not the only difference between the two systems. The two beams may have slight differences in geometry and/or material properties, for instance one may be longer than the other, or one may have a higher stiffness than the other. These differences were minimized by cutting each of the specimens from a common sheet of titanium, ensuring that each specimen was oriented with the grain of the sheet, and by cutting the sheet to the correct length before cutting strips off of the sheet to form the beams. So in this respect, the beams are as identical as can be expected. Other possible differences in the specimens occur at the upper support point where a thin string is fed through a small tube attached to the upper node of the beams and at the lower node where the permanent magnets are glued. The likely imperfections introduced at these locations could be from mislocation of the nodes, application of different amounts of glue, or using non-identical magnets. Fortunately, since differences occur at or near the nodes, the effect of these differences on the dynamics of the systems is negligible.

5. Conclusions

The method presented appropriately considers the material nonlinearities present and accurately captures the dependence of the stiffness and damping on a reference strain. This is accomplished using FEM based curvefits of the behavior of a coated beam and the experimentally measured system level properties of a coated and an uncoated beam. The results from this test are consistent with previous data sets and expand the knowledge of the behavior of these materials because these tests were performed over a wider strain range and used techniques that enabled a near continuous strain dependency to be found.

Acknowledgements

The author would like to acknowledge the support of the Turbine Engine Fatigue Facility to include Dr. Tommy George, Mr. Brian Runyon, US Air Force Research Laboratory, Wright Patterson Air Force Base, Ohio. Additionally, Mr. John Justice and Dr. Peter Torvik, Universal Technology Corporation, were instrumental in the analysis of material properties and the execution of the experiments. The research was funded by AFRL/TEFF and the Dayton Area Graduate Studies Institute.

References

[1] P.J. Torvik, Analysis of Free Layer Damping Coatings, Layered, Functional Gradient Ceramics, and Thermal Barrier Coatings, M. Anglada, E. Jiménez-Piqué and P. Hvizdoş, eds, *Key Engineering Materials* **333** (2007), 195–214..

[2] B. Runyon, T. George, C. Cross and P. Drew, *Automated Identification of Damping Material Properties*, 45th AIAA/ASME/ASCE/AHS/ASC Structures, Structural Dynamics and Materials Conference, Palm Springs, California, Apr. 19–22, 2004.

[3] S. Patsias, G.R. Tomlinson and A.M. Jones, Initial Studies into Hard Coatings for Fan Blade Damping, 6th National Turbine Engine High Cycle Fatigue (HCF) Conference, Jacksonville, Florida, 5–8 March, 2001.

[4] P.J. Torvik, S. Patsias and G.R. Tomlinson, *Characterizing the damping behavior of hard coatings: Comparisons from Two Methodologies*, 7th National Turbine Engine High Cycle Fatigue (HCF) Conference, Palm Beach Gardens, Florida, 14–17 May, 2002.

[5] S. Patsias, C. Saxton and M. Shipton, Hard Damping Coatings: an experimental procedure for extraction of damping characteristics and modulus of elasticity, *Journal of Materials Science and Engineering* **370** (2004), 412–416.

[6] D. Inman, *Engineering Vibration*, 2nd ed., Prentice Hall, Upper Saddle River, 2001.

[7] M. Simon and G.R. Tomlinson, Use of the Hilbert transform in modal analysis of linear and non-linear structures, *Journal of Sound and Vibration* **96**(4) (1984), 421–436.

[8] M. Feldman, Non-Linear Free Vibration Identification via the Hilbert Transform, *Journal of Sound and Vibration* **208**(3) (December 4, 1997), 475–489.

[9] N.O. Myklestad, Concept of Complex Damping, *Journal of Applied Mechanics* **19** (1952), 284–286.

[10] S. Reed, A.N. Palazotto and W. Baker, Evaluation of Strain Dependent Material Properties of Hard Coatings, *International Conference on Noise and Vibration Engineering* (2006), Leuven.

[11] P.J. Torvik, *Sources of Error in Obtaiing Damping Properties of Hard Coatings from Vibration Tests*, 76th Shock and Vibration Symposium, Shock and Vibration Information Analysis Center, Ft. Destin, 2005.

[12] S. Patsias and R. Williams, *Hard Damping Coatings: Material Properties and Finite Element prediction methods*, 8th National Turbine Engine High Cycle Fatigue (HCF) Conference, Monterey, California, 14th–16th April, 2003.

[13] P.J. Torvik, *General Tutorial on Damping: Part 3, Free Layer Damping Additions*, 75th Sound and Vibration Conference, 2004.

[14] P.J. Torvik, *Evaluation of Damping Properties of Coatings: Part I, Room Temperature*, prepared for Universal Technology Corporation, 2002.

[15] M. Shipton and S. Patsias, *Hard Damping Coatings: Internal Friction as the damping mechanism*, 8th National Turbine Engine High Cycle Fatigue (HCF) Conference, Monterey, California, 14th–16th April, 2003.

[16] P.J. Torvik, *Evaluation of Damping Properties of Coatings: Part I, Room Temperature*, prepared for Universal Technology Corporation, 2002.